MOLECULAR AND CELLULAR BIOLOGY, Dec. 2010, p. 5752–5763 Vol. 30, No. 24
0270-7306/10/$12.00 doi:10.1128/MCB.01147-10

Targeted Inactivation of *Mapk4* in Mice Reveals Specific Nonredundant Functions of Erk3/Erk4 Subfamily Mitogen-Activated Protein Kinases[▽]

Justine Rousseau,[1,3] Sonia Klinger,[1] Adeline Rachalski,[4,5] Benjamin Turgeon,[1,3] Paul Déléris,[1] Erika Vigneault,[4] Jean-François Poirier-Héon,[4,6] Maria Antonietta Davoli,[4] Naguib Mechawar,[4,5,6] Salah El Mestikawy,[4,5,6] Nicolas Cermakian,[4,5,6] and Sylvain Meloche[1,2,3]*

Institut de Recherche en Immunologie et Cancérologie[1] and Departments of Pharmacology[2] and Molecular Biology,[3] Université de Montréal, Montreal, Quebec H3C 3J7, Canada; Douglas Mental Health University Institute, Montreal, Quebec H4H 1R3, Canada[4]; and Departments of Psychiatry[5] and Neurology and Neurosurgery,[6] McGill University, Montreal, Quebec H3A 2T5, Canada

Received 29 September 2010/Accepted 8 October 2010

Erk4 and Erk3 are atypical members of the mitogen-activated protein (MAP) kinase family. The high sequence identity of Erk4 and Erk3 proteins and the similar organization of their genes imply that the two protein kinases are paralogs. Recently, we have shown that Erk3 function is essential for neonatal survival and critical for the establishment of fetal growth potential and pulmonary function. To investigate the specific functions of Erk4, we have generated mice with a targeted disruption of the *Mapk4* gene. We show that Erk4-deficient mice are viable and fertile and exhibit no gross morphological or physiological anomalies. Loss of Erk4 is not compensated by changes in Erk3 expression or activity during embryogenesis or in adult tissues. We further demonstrate that additional loss of Erk4 does not exacerbate the fetal growth restriction and pulmonary immaturity phenotypes of Erk3$^{-/-}$ mice and does not compromise the viability of Erk3$^{+/-}$ neonates. Interestingly, behavioral phenotyping revealed that Erk4-deficient mice manifest depression-like behavior in the forced-swimming test. Our analysis indicates that the MAP kinase Erk4 is dispensable for mouse embryonic development and reveals that Erk3 and Erk4 have acquired specialized functions through evolutionary diversification.

Mitogen-activated protein (MAP) kinases are core components of evolutionarily conserved signaling pathways that play a key role in eukaryotic signal transduction. These enzymes process information from a wide variety of extracellular stimuli and cellular perturbations to control multiple physiological processes required to maintain normal cellular and tissue homeostasis (4, 6, 13, 26, 41). The MAP kinase family is composed of seven distinct subfamilies in mammals: Erk1/Erk2, Jnk1/2/3, p38α/β/δ/γ, Erk5, Erk3/Erk4, Nlk, and Erk7 (4). Among these, Erk4 remains the least characterized member of the family.

Erk4 (originally known as p63^{mapk}) is a 70-kDa protein kinase that is most closely related to the MAP kinase Erk3, with 73% amino acid identity within the kinase catalytic domain (1, 10). In addition to their kinase domain located at the N terminus, the two proteins contain a noncatalytic C-terminal region of unknown function. The first 150 residues of the C-terminal extension display nearly 50% identity between the two kinases, whereas the extreme C terminus differs both in length and in sequence. Erk4 and Erk3 also contain a single phosphoacceptor site (SEG) in the activation loop and the unique sequence SPR instead of APE in subdomain VIII of the kinase domain, two features that distinguish them from other MAP kinases. At the genomic level, the genes encoding Erk4 (*Mapk4*) and Erk3 (*Mapk6*) share a similar organization of exon/intron boundaries, suggesting that they arose by duplication of a common ancestor (37). All these observations imply that Erk4 and Erk3 are true paralogous proteins.

The cellular and physiological functions of Erk4 remain to be defined. Erk4 and Erk3 have a more restricted substrate specificity than conventional MAP kinases like Erk1/2, Jnk, or p38, and their only substrate identified thus far is the MAP kinase-activated protein kinase MK5 (1, 7, 15, 31, 33). Little is known about either the upstream signals that control the expression and/or activity of the two kinases. In a recent study, we reported the phenotype of Erk3-deficient mice (18). Loss of Erk3 function leads to intrauterine growth restriction, associated with delayed lung maturation and early neonatal lethality. These findings indicate that Erk3 exerts specialized functions in certain tissues or, alternatively, that Erk3 and Erk4 display tissue-specific patterns of expression. To investigate the specific function of Erk4 and to further characterize the role of Erk3/Erk4 MAP kinase subfamily in mouse development, we have generated mice with a disruption of the *Mapk4* gene. We show that Erk4-deficient mice are viable and fertile and develop normally. The absence of Erk4 is not compensated by changes in Erk3 expression or activity, and the additional loss of Erk4 in Erk3-deficient embryos does not accentuate Erk3 phenotypes. However, behavioral characterization of Erk4$^{-/-}$ adult mice revealed an increased depression-like behavior. Our

* Corresponding author. Mailing address: Institut de Recherche en Immunologie et Cancérologie, Université de Montréal, 2950, chemin de Polytechnique, Montreal, Quebec H3T 1J4, Canada. Phone: (514) 343-6966. E-mail: sylvain.meloche@umontreal.ca.

▽ Published ahead of print on 18 October 2010.

results suggest that Erk3 and Erk4 paralogs have evolved specific functions and indicate that Erk3 plays a more prominent role in mouse embryogenesis.

MATERIALS AND METHODS

Targeting strategy and generation of *Mapk4*-deficient mice. The targeted region of the *Mapk4* gene was isolated from a mouse 129Sv genomic library in λGEM12 bacteriophage. Identification of positive clones was done by plaque purification using a ^{32}P-labeled probe derived from exon 2 of *Mapk4* (Mouse Genome Informatics database accession no. 2444559). Homologous genomic fragments of 3.5 kb and 2.5 kb flanking exon 2 (encoding amino acids 1 to 182) were amplified by PCR with primers. For the 3.5-kb genomic fragments flanking exon 2, the forward primer 5′-CCG GAA TTC CTT CAA GAA ACT CCA GCT C-3′ and reverse primer 5′-CCG GAA TTC TCA GCC ATT GTT GCC TCA G-3′ (5′ fragment) were used. For the 2.5-kb genomic fragments flanking exon 2, the forward primer 5′-CGG ACT AGT GGG TGT CTT CAT CAT CCT CTC-3′ and reverse primer 5′-CGG ACT AGT CCT ACT AAG AGG AGT GGC AG-3′ (3′ fragment) were used. The two genomic fragments were subcloned into pBluescript vector. Exon 2 coding sequence was replaced by the green fluorescent protein (GFP) reporter gene containing a polyadenylation signal and inserted in frame at the initiation codon of Erk4 (see Fig. 1A). The neomycin (Neo) resistance cassette was inserted 3′ of the GFP gene. The targeting vector was linearized by NotI digestion and electroporated in R1 embryonic stem (ES) cells (22). ES cell clones that underwent homologous recombination at the *Mapk4* locus were identified by Southern blot analysis (see below). Two correctly targeted ES clones (clones 117 and 148) were injected into C57BL/6 blastocyst-stage embryos. Chimeric males were bred with C57BL/6 female mice, and germ line transmission was confirmed by Southern blot analysis. F1 heterozygotes were intercrossed to generate homozygous mutant animals.

Genotyping of ES cells and mice. For screening of ES cells, DNA was digested with KpnI, and the recombinant *Mapk4* allele was identified by Southern blot analysis. Correct genomic integration of the construct was verified using a 5′ external probe and a 3′ internal probe corresponding to the Neo gene (see Fig. 1A). The 5′ probe was generated by PCR using the following primers: forward, 5′-ATGTGACTCAGCTGCTTG-3′; and reverse, 5′-CTC AGA ACT CCG GTG AGT-3′. The presence of the mutated allele was confirmed by the appearance of a 6.8-kb or 5.1-kb fragment, respectively.

Mapk4 mutant mice were genotyped by PCR. The presence of the wild-type allele was confirmed by amplification of a 689-bp fragment containing exon 2 coding region using the following primers: forward, 5′-TTG ACT TCC AAC CCC TTG GC-3′; and reverse, 5′-ATT GGC CAA AGG CAT GTG GC-3′. The mutated allele was identified by amplification of a 422-bp fragment specific to the GFP gene using the following primers: forward, 5′-TCT TCT TCA AGG ACG ACG GC-3′; and reverse, 5′-CTT GTA CAG CTC GTC CAT GC-3′.

Mouse husbandry and experimentation. *Mapk6* mutant mice have been described previously (18). Animals were housed under specific-pathogen-free conditions and were handled in accordance with the procedures and protocols approved by the Université de Montréal and McGill University institutional animal care committees. Mice maintained on a mixed C57BL/6J × 129/Sv genetic background were used for initial phenotypic characterization, histopathological analysis, and growth studies. Brain *in situ* hybridization, neurogenesis, and behavioral experiments were conducted in congenic C57BL/6J *Mapk4* mutant mice (backcrossed to C57BL/6J strain for more than 10 generations). When indicated the beginning of gestation (embryonic day 0.5 [E0.5]) was confirmed by the presence of a vaginal plug. Embryos were removed by caesarean section.

Primary cell culture and proliferation assays. Mouse embryonic fibroblasts (MEFs) were prepared from E14.5 embryos isolated from crosses of *Mapk4* and *Mapk6* mutant mice on a congenic C57BL/6J background. The cells were cultured in Dulbecco's modified Eagle medium (DMEM) supplemented with 10% newborn calf serum and antibiotics (39).

Cell proliferation was measured by the colorimetric 3-(4,5-dimethylthiazol-2-yl)-2,5-diphenyltetrazolium bromide (MTT) assay using primary MEFs at early passages as previously described (39).

Immunoblotting analysis and kinase assay. Antibodies were from the following sources: polyclonal anti-Erk3 (4067) was from Cell Signaling Technology, polyclonal anti-GFP (G8965-05-1) was from US Biological, and polyclonal anti-glyceraldehyde-3-phosphate dehydrogenase (anti-GAPDH) (sc-25778) was from Santa Cruz Biotechnology. Polyclonal antibody to the C terminus of Erk4 was described previously (7). For immunoblotting analysis, adult tissue proteins were extracted by homogenization of 8-week-old mouse tissues as previously described (38). Lysates of MEFs were prepared as described previously (32). Lysate proteins (200 μg) were resolved by SDS-polyacrylamide gel electrophoresis and transferred onto Hybond-C nitrocellulose membranes. The membranes were immunoblotted with anti-Erk3 (1:750), anti-Erk4 (1:1,000), and anti-GAPDH (1:1,000) primary antibodies. Immunoreactive bands were detected by enhanced chemiluminescence.

The *in vivo* kinase activity of endogenous Erk3/Erk4 was evaluated by measuring their ability to increase the Hsp27 kinase activity of recombinant MK5 in a coupled kinase assay. Brain protein extracts (7 mg protein) were incubated for 4 h at 4°C with 2 μg of recombinant His_6-MK5-GST (GST stands for glutathione *S*-transferase) (7) immobilized on gluthatione-agarose beads (Amersham). Erk3/Erk4-MK5 complexes were pulled down, and the phosphotransferase activity of MK5 was assayed as previously described (7) using 2 μg of p38-regulated/activated protein kinase (PRAK) substrate peptide (Millipore) as a substrate. The reaction was stopped by transferring the mixture onto P81 paper (Millipore). The papers were washed extensively in 1% phosphoric acid, and the radioactivity content was quantified in a liquid scintillation counter.

RNA extraction and quantitative reverse transcription-PCR (RT-PCR). Total RNA from embryos at different developmental stages was extracted by homogenizing the whole embryo in RLT buffer and subsequently purified using the RNeasy kit (Qiagen) according to the manufacturer's specifications. The integrity of the RNA was confirmed by analysis with the Agilent 2100 bioanalyzer using the eukaryote total RNA nano assay. RNA was reverse transcribed using the high-capacity cDNA archive kit (Applied Biosystems) with random primers. Real-time PCR amplification was detected using the ABI PRISM 7900HT fast sequence detection system (Applied Biosystems). *Mapk4* transcription was monitored using the following primers and probe: forward primer, 5′-GGACGTCA ACAGTGAAGCCATTGA-3′; reverse primer, 5′-TCGATCTCGTCCTCAAT GCGGAAA-3′; and internal probe, 5′-TCAGCATCCTTACATGAGCCCGTA CT-3′. *Mapk6* transcription was monitored using the following: forward primer, 5′-AACGACATGACTGAGCCACACAGA-3′; reverse primer, 5′-TGTAAGG ATGGGAAAGGGCTTCCT-3′; and internal probe, 5′-ATCAGCCGAGAAG CACTGGATTTCCT-3′. All reactions were run in triplicate, and the average value was used for quantification. Hypoxanthine guanine phosphoribosyl transferase (HPRT) was used as endogenous control. Real-time PCR efficiencies were calculated for each gene: the values were 1.8791 for *Mapk4*, 1.8825 for *Mapk6*, and 2.1435 for HPRT. The PCR efficiency for each gene was taken into consideration for calculation of the relative expression ratio as described by Pfaffl and Roche Diagnostics mathematical models (27).

Histology analysis. Tissues from E18.5 embryos and 8-week-old adult mice were fixed overnight in 10% formalin, embedded in paraffin, and sectioned at 5-μm thickness. Tissue sections were stained using conventional hematoxylin and eosin protocol. Lung sections were also stained with periodic acid-Schiff (PAS). For quantitative morphometric analysis, PAS-positive cells, tissue area, and saccular airspace were measured with the Image ProPlus software on 10 randomly selected micrographs.

In situ hybridization. Adult Erk4$^{+/+}$ and Erk4$^{-/-}$ mice (10 to 12 weeks old) were sacrificed by cervical dislocation, and their brains were removed and frozen in isopentane at −30°C. Sagittal sections were prepared with a cryostat at −20°C, thaw mounted on glass slides, and stored at −80°C until analysis. The pattern of Erk4 mRNA expression was determined by *in situ* hybridization with α-^{35}S-dATP-labeled oligonucleotides as previously described (11). Antisense probes were designed from the mouse *Mapk4* sequence (GenBank accession number NM_172632) to target different regions of Erk4 mRNA. Five specific probes were generated using the following sequences: Erk4-1 (starts at nucleotide [nt] 186 of the *Mapk4* sequence [GenBank accession number NM_172632), 5′-GAC ATC CTC TTT CAC CCA CTT ATC TGC AGC ACC TT-3′; Erk4-2 (starts at nt 235 of the *Mapk4* sequence), 5′-TAC AAA AAG AAC TCA GCT GCC AGG CCA GGA CCC TT-3′; Erk4-3 (starts at nt 709 of the *Mapk4* sequence), 5′-TGC TAA GGT TGT TGT TAC CTG CAC TTG GAG GGT TT-3′; Erk4-4 (starts at nt 2428 of the *Mapk4* sequence), 5′-ATG CAC GCG CCA TTC AGG TCG CCC AGT TTG TTT TC-3′; and Erk4-5 (starts at nt 2863 of the *Mapk4* sequence), 5′-GCT CCC AGA GGT TAA AGG CTA GTT ATT TAG GCA GT-3′. Oligonucleotides were labeled with α-^{35}S-dATP (Perkin Elmer) using terminal transferase (Promega) to a specific activity of 5×10^8 cpm/μg. Brain sections were fixed with 3.7% formaldehyde in phosphate-buffered saline (PBS), washed with PBS, rinsed with water, dehydrated with 70% ethanol, and air dried. Sections were then covered with 100 μl of hybridization medium containing Helios buffer (Helios Biosciences) and 4×10^6 cpm of labeled probe mix. The slides were incubated overnight at 42°C, stringently washed, and dried. The slides were mounted and exposed to BAS-TR Fuji imaging screens (Fuji Film Photo). The screens were then scanned with a Fuji bioimaging analyzer BAS-5000 (Fuji Film Photo). Labeled probes were tested for the hybridization step individually or pooled together. Negative controls were performed using labeled probe

Erk4-4 on Erk4$^{-/-}$ mouse brain sections. The expression pattern was compared to the Paxinos and Franklin mouse brain atlas (25).

Neurogenesis analysis. Twelve-week-old mice were injected four times intraperitoneally (i.p.) with 50 mg of 5′-bromo-2′-deoxyuridine (BrdU) per kg of body weight over the course of 10 h and sacrificed 20 days later. The animals were anesthetized by i.p. injection of ketamine-xylazine and perfused first with PBS and then with 4% paraformaldehyde in 0.1 M phosphate buffer. The brains were then removed, postfixed in fixative overnight at 4°C, cryoprotected in a sucrose solution, and cut on a freezing microtome into serial 40-μm-thick coronal sections. The sections were stored in a cryoprotectant solution (30% glycerol, 30% ethylene glycol, 40% PBS) at −20°C until further use. For BrdU immunocytochemistry, the sections were permeabilized with 0.2% Triton X-100 in PBS for 90 min, followed by treatment with 0.9% H_2O_2 in PBS for 10 min to block endogenous peroxidase. DNA was denatured in 2 M HCl in PBS for 30 min at 37°C. The sections were washed, blocked in PBS containing 2% normal goat serum and 0.2% Triton X-100 for 30 min, and incubated overnight with primary rat anti-BrdU antibody (140207; Serotec) (1:1,000). After the slides were washed with PBS, they were incubated for 2 h with anti-rat IgG secondary antibody (S0928; Vector Laboratories) (1:200). For double-cortin (DCX) staining, the sections were blocked as described above before incubation in goat anti-DCX antibody (F1307; Santa Cruz) (1:1,000) followed by anti-goat IgG secondary antibody (U0111; Vector Laboratories) (1:200). In both cases, staining was revealed using the Vectastain Elite ABC system (Vector Laboratories). The number of immunoreactive cells was quantified by light microscopy (Leica DM2500) at a magnification of ×20 from series of alternate sections, in the dentate gyrus and olfactory bulb (granule cell layer and glomerular layer).

Motor performance and behavioral tests. Performance and behavioral testing was conducted on male adult mice (3 to 4 months of age) between 9:00 a.m. and 3:00 p.m. Each test was performed at the same hour for all groups, and an interval of 3 and 8 days was allowed between two successive series of tests. The tests were performed by an observer who was unaware of the mouse genotype.

(i) SLA. Spontaneous locomotor activity (SLA) was assessed by using a Versamax animal activity monitor (AccuScan Instruments Inc.) with laser beams placed on the Plexiglas chamber's side to detect animal movements. Mice were placed randomly and individually into Plexiglas actimeter chambers (40 by 40 by 39 cm). The lights were shut off, and the mice were allowed 30 min of habituation in the chamber before a 60-min period of measurements. Activity was monitored as the number of laser beam breaks per 10 min. The following measures were collected: total distance, total activity time, and total time for stereotypic movements.

(ii) Motor coordination. Motor coordination and equilibrium were tested on an accelerating rotarod (IITC Life Science). Mice were placed on a rotating rod and were first trained on the apparatus for four trials at an interval of 30 min. The speed of the rotation was gradually increased from 4 to 24 rpm during the trials. The next day, mice were replaced on the rotarod for the four trial tests at a constant speed of 25 rpm. Maximal time on the rotating rod, maximal speed, and total distance were recorded for a maximum of 5 min.

(iii) Spatial memory. Spatial memory was analyzed by the Morris water maze task (21). The test was conducted in a white circular swimming pool (140 cm in diameter and 140 cm deep) filled with 30 cm of opaque water maintained at 24°C. Three spatial cues were spread at equal distance on the pool walls and remained in the same location with respect to the pool. A square Plexiglas platform was positioned 0.5 cm below the surface of the water in the center of a defined quadrant of the maze. Animal movements were recorded using a video camera fixed to the ceiling of the room and connected to the Water 2100 software (HSV Image). During four consecutive days (learning stage), each mouse was subjected to a series of four trials. Each trial consisted of releasing the mouse into the water facing the wall of the pool at different cardinal points, randomly distributed. Mice were allowed a period of 60 s to find the platform, and animals that failed to locate it were placed onto the platform by the experimenter and were held there for 15 s before they were returned to their home cage. On day 5, a probe trial was performed, in which the platform was removed and the mouse was allowed to swim for a fixed duration of 60 s. The length of time to reach the platform, the path length, and the swimming speed were recorded for each trial.

(iv) Anxiety-related behavior. Anxiety-related behavior was tested in two different paradigms: elevated plus maze and Thatcher-Britton test (28). The elevated plus maze consisted of two opposing open arms (30 by 5 cm) and two opposing closed arms (12 cm high) of the same size shaped in the form of a plus sign and elevated 50 cm from the floor. Each mouse was placed into the center area of the maze (5 by 5 cm) facing a closed arm. The mice were allowed to explore the maze for 5 min. The time spent in the open arms of the maze and the number of entries into the open arms were analyzed. For the Thatcher-Britton test, mice were deprived of food for 24 h, and placed along one wall of an open-field apparatus (60 by 60 by 50 cm) with 12 pellets of standard mouse chow placed in the center of the open field. The latent period to begin eating (not only sniffing or manipulating the pellet) was measured.

(v) Depression-related behavior. Depression-like behavior was assessed using the forced-swimming test paradigm (16). Mice were plunged during 6 min in a 30- by 12-cm beaker filled with 20 cm of water at 24°C. After each session, the mouse was removed and allowed to dry. Depression-like behavior was measured as the amount of immobility (making only minimal movements to keep the head above water and floating) measured during the last 4 min of the session (after a period of 2 min of habituation).

Statistical analysis. Results are expressed as the means ± standard errors of the means (SEMs). Unpaired *t* test was performed unless otherwise indicated. Sessions in the Morris water maze were analyzed by repeated-measure analysis of variance (ANOVA) (GraphPad Prism).

RESULTS

Generation of Erk4-deficient mice. To inactivate the *Mapk4* gene encoding Erk4, we deleted the genomic sequence coding for amino acids 1 to 182 in exon 2 by inserting the GFP gene in frame with the initiation codon. Replacement of exon 2 by the GFP reporter gene containing a stop codon and a polyadenylation signal is predicted to generate a null allele (Fig. 1A). To identify the mutated allele and confirm the correct genomic integration at the *Mapk4* locus, we inserted a KpnI restriction site in the targeting vector to generate new fragments of 6.8 kb and 5.1 kb upon digestion. Two correctly targeted ES clones (Fig. 1B) were independently injected into blastocysts to generate chimeric mice. Both clones transmitted the mutant allele to the germ line and were used to generate heterozygous and homozygous *Mapk4* mutant mice (Fig. 1C). Western blot analysis confirmed that no Erk4 protein expression was detectable in extracts of Erk4$^{-/-}$ MEFs prepared from the litters of heterozygous intercrosses (Fig. 1D).

Erk4-deficient mice are viable and fertile and exhibit no gross physiological abnormalities. Genotype analysis of the offspring from crosses of Erk4$^{+/-}$ mice confirmed the presence of viable Erk4-deficient mice at weaning (Fig. 1C). To determine whether the loss of Erk4 has any effect on mouse viability, we analyzed the genotype distribution of Erk4$^{+/-}$ intercross progeny generated from the two different ES clones. Inheritance of the mutated allele at the expected Mendelian frequency (Table 1) confirmed the absence of embryonic or neonatal lethality in Erk4 mutant progeny. Erk4-deficient male and female mice were similarly distributed in the progeny (Table 1) and found to be fertile, as indicated by their ability to generate litters of normal size (data not shown). Gross examination of Erk4$^{-/-}$ mice revealed no obvious growth defect or morphological anomalies compared to wild-type littermates. Likewise, a complete histopathological analysis did not reveal any structural abnormality in mutant mice (Table 2). These results show that Erk4 is dispensable for embryonic and postnatal development.

We performed initial studies to assess the impact of Erk4 deficiency on cell proliferation *in vitro*. Primary MEFs were prepared from E14.5 Erk4$^{-/-}$ and wild-type littermate embryos in a congenic C57BL/6J background and analyzed at primary passage 3 (P3). The morphology of Erk4$^{-/-}$ MEFs was comparable to that of wild-type control cells (data not shown). No difference in the proliferation rate of Erk4-deficient fibroblasts and wild-type cells was observed in cells grown in either 10% serum (Fig. 2A) or low-serum (3% serum) (data

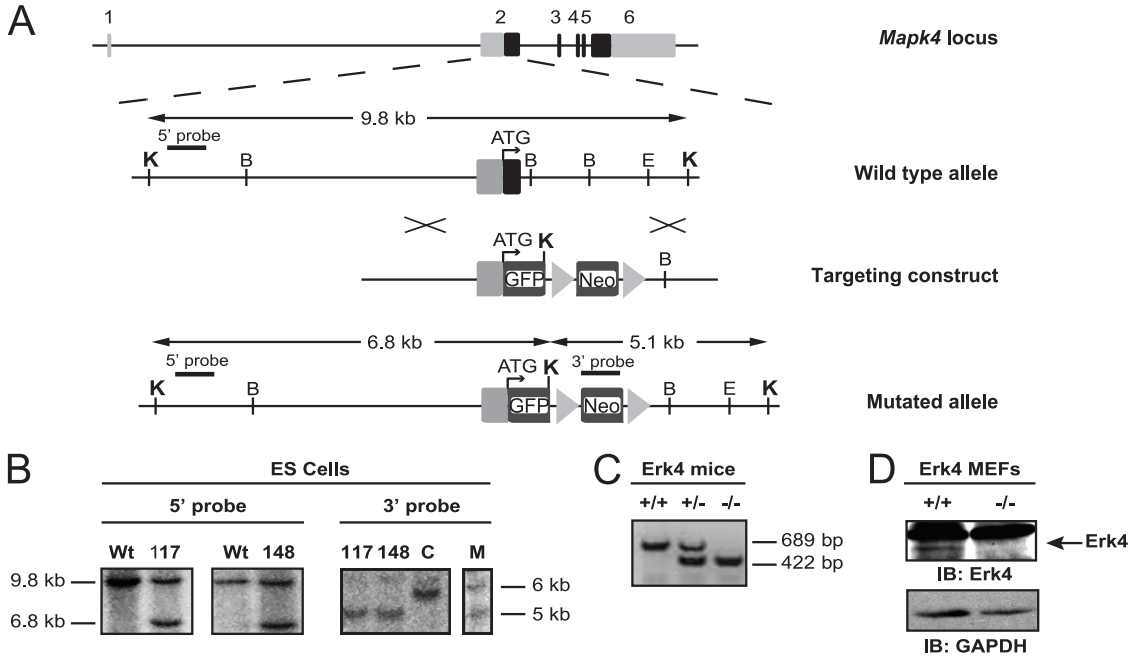

FIG. 1. Generation of Erk4-deficient mice. (A) Schematic representation of the *Mapk4* locus, wild-type allele, targeting vector, and mutated allele. Exons 1 to 6 are represented by numbered gray or black bars or boxes. Gray bars or boxes represent untranslated regions (UTRs), and black bars or boxes represent coding regions. The targeting vector carries a neomycin resistance gene (*Neo*) and the GFP reporter gene fused in frame with the *Mapk4* coding sequence initiation codon. A KpnI restriction site was inserted in the GFP gene to facilitate identification of the mutated allele. The positions of KpnI (K), BamHI (B), and EcoRI (E) restriction sites are shown. (B) Southern blot analysis of KpnI-digested genomic DNA from two correctly targeted ES clones (clones 117 and 148): 5′ probe, wild-type (Wt) allele (9.8 kb) and mutant allele (6.8 kb); 3′ probe, mutant allele (5.1 kb). Lanes: C, randomly integrated control; M, 1-kb marker. (C) PCR analysis of genomic DNA from 3-week-old $Erk4^{+/-}$ intercross progeny. (D) Immunoblot (IB) analysis of Erk4 protein expression in total cell extracts of $Erk4^{+/+}$ and $Erk4^{-/-}$ mouse embryonic fibroblasts (MEFs).

not shown) conditions. Additional inactivation of the paralogous gene encoding Erk3 did not compromise the proliferation of embryonic fibroblasts (Fig. 2B). These results indicate that Erk4 activity is not required for the proliferation of fibroblasts under normal physiological conditions.

Loss of Erk4 is not compensated by changes in Erk3 expression or kinase activity. Erk4 is a paralog of Erk3, and both kinases are coexpressed in brain, lung, kidney and other tissues during mouse embryogenesis (15). We evaluated the possibility that loss of Erk4 could be compensated by changes in Erk3 expression and/or activity. We first measured the expression of Erk3 and Erk4 transcripts during embryonic development by quantitative RT-PCR. The level of Erk3 mRNA in whole embryos was the highest at E11.5 (Fig. 3A), as previously shown by Northern blot analysis (38). Interestingly, the Erk4 gene displayed a similar temporal expression pattern with a marked upregulation at E11.5 (Fig. 3A). We next measured the expression levels of Erk3 mRNA in Erk4-deficient embryos. Compared to wild-type animals, no increase in Erk3 mRNA level was detected in $Erk4^{-/-}$ embryos at any embryonic day (Fig. 3B). We then analyzed the expression of Erk3 and Erk4 proteins in various adult mouse tissues by immunoblot analysis.

TABLE 1. Genotype and sex distribution analysis of the progeny from $Erk4^{+/-}$ intercrosses[a]

$Erk4^{+/-}$ intercross progeny[b]	Total no. of pups	No. of pups (%) with the following genotype:			No. of pups (%)	
		Erk4$^{+/+}$	*Erk4*$^{+/-}$	*Erk4*$^{-/-}$	Male	Female
Clone 117	117	27 (23)	64 (55)	26 (22)	60 (51)	57 (49)
Clone 148	108	31 (29)	46 (43)	31 (29)	61 (56)	47 (44)

[a] Progeny with C57BL/6J–129/Sv mixed genetic background.
[b] $Erk4^{+/-}$ intercross progeny generated from the two independent ES clones.

TABLE 2. Histopathological analysis of Erk4 knockout mice

Organ or tissue	Result of histopathological analysis
Brain	Normal
Kidney	Normal
Heart	Normal
Lung	Normal
Spleen	Normal
Liver	Normal
Striated muscle	Normal
Pancreas	Normal
Colon	Normal
Bone marrow	Normal
Testis	Normal
Thymus	Normal
Spinal cord	Normal
Gallbladder	Normal
Urinary bladder	Normal
Small bowel	Normal
Large bowel	Normal
Skin	Normal
Fat tissue	Normal

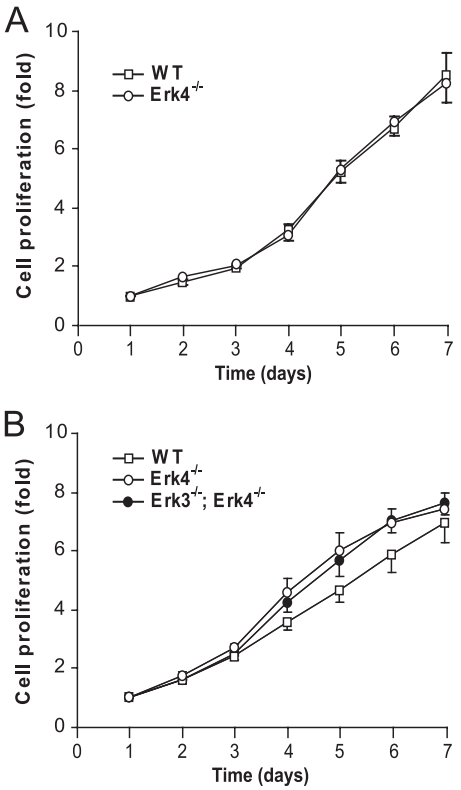

FIG. 2. Absence of Erk4 does not affect the proliferation rate of primary MEFs. (A) The proliferation rate of passage 3 (P3) MEFs prepared from *Mapk4*$^{-/-}$ or wild-type (WT) littermate embryos was measured by the MTT assay. Values are expressed as fold increase in cell number and correspond to the means ± standard errors of the means (SEMs) (error bars) of 7 or 8 independent MEF preparations. (B) Proliferation curves of MEFs isolated from *Mapk4*$^{-/-}$ embryos, *Mapk4*$^{-/-}$; *Mapk6*$^{-/-}$ embryos, or wild-type embryos.

We found that Erk4 protein is expressed at the highest level in the brain and at lower levels in the kidney, heart, lung, and stomach (Fig. 3C). In accordance with previous data showing a broad expression pattern of Erk3 mRNA (38), Erk3 protein was detected in most tissues of wild-type animals (Fig. 3D). When we measured Erk3 levels in the tissues of Erk4$^{-/-}$ mice, we observed no change in Erk3 expression compared to Erk4$^{+/+}$ tissues (Fig. 3D). These results indicate that loss of Erk4 is not compensated by changes in Erk3 expression during embryonic development or adult life in mice.

To address whether changes in Erk3 kinase activity could compensate for the loss of Erk4, we measured global Erk3/Erk4 activity in the brains of Erk4$^{+/+}$ and Erk4$^{-/-}$ mice. Erk3 and Erk4 were pulled down from brain extracts with His_6-MK5-GST, and their activity was assayed by monitoring the catalytic activation of MK5 in a coupled enzymatic assay. The activation of MK5 was decreased by 50% in the absence of Erk4, suggesting that changes in Erk3 activity do not compensate for the loss of Erk4 protein (Fig. 3E).

Expression of Erk4 mRNA in adult mouse brain. Given the predominance of Erk4 expression in brain tissue (Fig. 3C), we wanted to determine the precise spatial distribution of Erk4 mRNA in the adult mouse brain by *in situ* hybridization. Five specific probes targeting different regions of the mRNA were designed to ascertain the pattern of expression of Erk4 in sagittal brain sections. All the probes generated a similar expression pattern (data not shown). Figure 4A shows typical sagittal sections of adult mouse brain hybridized with a mix of Erk4 probes. Strong but discrete labeling was present in a number of structures of the forebrain. Erk4 mRNA is strongly expressed in the granule cell and in the external plexiform layers of the olfactory bulb, in layer two of the cerebral cortex, in piriform cortex, in olfactory tubercle, and in the nucleus accumbens and caudate putamen sectors of the striatum. The Erk4 hybridization signal is also apparent in the dorsal and ventral parts of the lateral ventricle and in the lateral recess of the fourth ventricle. In the hippocampus, high expression was detected in the CA1 region, in the granular layer of the dentate gyrus, and in the postsubiculum. Erk4 mRNA expression is also found in deep cerebellar nuclei, pontine nuclei, principal sensory trigeminal nucleus, and spinal trigeminal tract. Erk4 signal is absent in the internal capsule and in the inferior cerebellar peduncle, which are white matter structures. No significant hybridization signal was detected in sagittal brain sections from Erk4$^{-/-}$ mice (Fig. 4B).

Adult brain neurogenesis is not affected by the loss of Erk4. Adult neurogenesis occurs throughout life in the mammalian dentate gyrus and the olfactory bulb (3). Given the high level of expression of Erk4 mRNA in these two areas of the brain, we evaluated the possible implication of Erk4 in brain neurogenesis. The number of BrdU- and DCX-immunoreactive cells, reflecting cell replication and immature neurons, respectively, was counted in each of the neurogenic regions (dentate gyrus of the hippocampus, and granule cell layer and glomerular layer of the olfactory bulb). No significant difference was found between the genotypes (Fig. 5).

Behavioral characterization of Erk4-deficient mice. The locomotor activity and motor coordination of mice were analyzed using the actimetry and rotarod tests. Erk4$^{-/-}$ mice did not differ from wild-type littermate controls in the total distance traveled ($P = 0.42$) and time spent in movement ($P = 0.43$) in the actimeter chamber (Table 3). We also monitored the time spent in stereotypic movements as an indicator of motor defects and found no difference between Erk4 mutant and wild-type animals ($P = 0.11$) (Table 3). The rotarod test was used to assess the motor coordination of mice. No significant difference in the maximal time on cylinder ($P = 0.78$), maximal speed ($P = 0.70$), and traveled distance ($P = 0.87$) was found between Erk4$^{-/-}$ and Erk4$^{+/+}$ mice (Table 4). These results suggest that locomotor activity, motor coordination, and equilibrium are not affected by the absence of Erk4.

The expression of Erk4 mRNA in the hippocampus and lateral ventricle prompted us to investigate the impact of Erk4 deficiency on spatial learning and memory performance in the Morris water maze paradigm. Mice were trained during 4 days with the hidden platform. No change in the learning capacity of Erk4$^{-/-}$ mice could be observed compared to control animals ($F_{(1,40)} = 0.72$; $P > 0.05$) (Fig. 6A). In the probe test, both wild-type and Erk4$^{-/-}$ mice spent a similar percentage of time selectively searching inside the target quadrant ($P = 0.20$) (Fig. 6B).

The anxiety-like behavior of Erk4 mutant mice was evaluated using the elevated plus maze and Thatcher-Britton tests. No significant difference in the time spent in open arms ($P =$

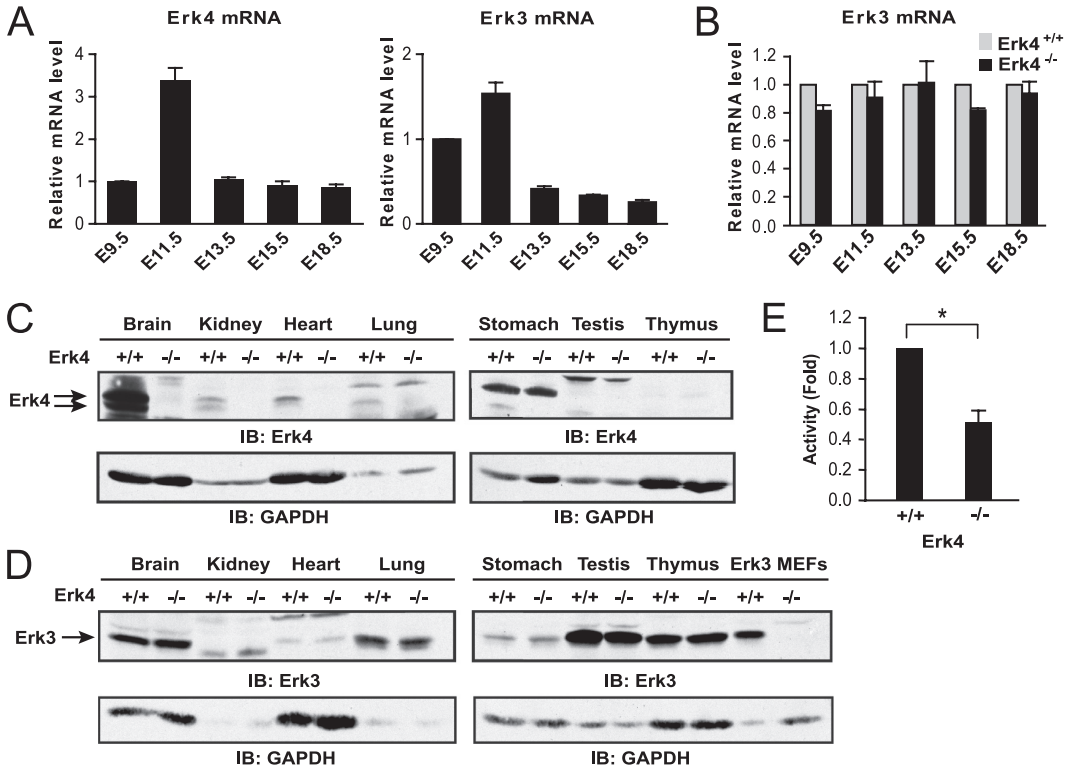

FIG. 3. Absence of Erk4 is not compensated by changes in Erk3 expression or activity. (A and B) mRNA expression during embryonic development. Total RNA was extracted from wild-type or Erk4$^{-/-}$ whole embryos at different embryonic stages. Expression of Erk4 and Erk3 mRNA was analyzed by quantitative RT-PCR. (A) Levels of Erk3 and Erk4 mRNA in wild-type mice are expressed as fold difference relative to mRNA expression at E9.5 and represent the means plus SEMs (error bars) ($n = 3$). (B) Levels of Erk3 mRNA in Erk4$^{-/-}$ embryos are expressed relative to their expression levels in Erk4$^{+/+}$ embryos at the corresponding embryonic day (E9.5 to E18.5). Values are means plus SEMs ($n = 3$). (C and D) Protein expression in adult tissues. Total proteins were extracted by homogenization of whole tissues from 8-week-old wild-type and Erk4$^{-/-}$ littermates, and equal amounts of proteins were resolved by SDS-polyacrylamide gel electrophoresis. Expression of Erk4 (C) and Erk3 (D) was analyzed by immunoblotting (IB) with specific antibodies. Cellular extracts of Erk3$^{+/+}$ and Erk3$^{-/-}$ MEFs were used as control to show the specificity of Erk3 antibody. The specificity of anti-Erk4 antibody is presented in Fig. 1D. (E) Kinase activity. Protein extracts from Erk4$^{+/+}$ and Erk4$^{-/-}$ brains were incubated for 4 h at 4°C with recombinant His_6-MK5-GST. Erk3/Erk4-MK5 complexes were pulled down, and the phosphotransferase activity of MK5 was measured in a coupled assay using PRAK substrate peptide as the substrate. Results are expressed as fold change in activity and represent the means plus SEMs of 3 experiments. The values for kinase activity for Erk4$^{+/+}$ and Erk4$^{-/-}$ mice are significantly different ($P < 0.05$) as indicated by the asterisk and bracket.

0.28) in the elevated plus maze paradigm or latent period to begin eating ($P = 0.23$) in the Thatcher-Britton test was observed between Erk4$^{-/-}$ and wild-type animals (Table 5).

Depression-like behavior was analyzed using the forced-swimming test. In this paradigm, an increased floating time is considered to be a measure of resignation to escape from aversive stimulus, which is indicative of depression-related behavior. We found that Erk4$^{-/-}$ mice manifest an increased immobility time ($P < 0.01$) compared to control animals, suggesting that loss of Erk4 accentuates depression-related behavior (Fig. 7).

Loss of Erk4 function does not accentuate Erk3-deficient mouse phenotypes. We recently reported that inactivation of the paralogous kinase Erk3 results in intrauterine growth restriction, pulmonary immaturity, and neonatal lethality (18). To address the question of functional redundancy between Erk4 and Erk3 during embryogenesis, we sought to determine whether loss of Erk4 accentuates the phenotypes of Erk3-deficient mice. Erk3-deficient mice display significant growth restriction at birth with a reduction (25 to 40%) of fetal lung, heart, and liver weight (18). In addition, Erk3 null mice exhibit a lung maturation defect characterized by decreased saccular space and increased glycogen content of type II pneumocytes. To evaluate the contribution of Erk4 to these phenotypes, we first measured the body weight and the weight of the heart and the lung in the progeny of Erk4$^{+/-}$ intercrosses at E18.5. No reduction in body weight or decrease in fetal heart and lung weights was observed in Erk4$^{-/-}$ embryos compared to their wild-type littermates (Fig. 8A and B). To look into a possible lung maturation defect, we quantitatively measured the lung saccular space and glycogen content of type II pneumocytes in Erk4$^{+/-}$ intercross progeny at E18.5. Histological analysis of hematoxylin-and-eosin-stained lung sections revealed normal saccular space in Erk4$^{-/-}$ animals (Fig. 8C and D). By staining lung sections with PAS, we found no difference in intracellular glycogen content of type II pneumocytes between wild-type and Erk4 mutants (Fig. 8C and E). These results indicate that loss of Erk4 does not alter intrauterine growth and lung maturation and suggest that Erk3 exerts specific functions in these tissues during embryogenesis.

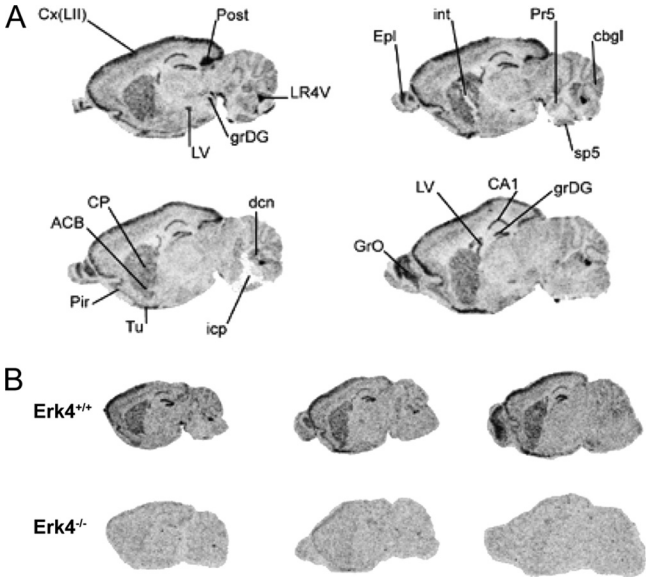

FIG. 4. Distribution of Erk4 mRNA in adult mouse brain. (A) Expression of Erk4 mRNA was analyzed by *in situ* hybridization on mouse brain sagittal sections (from Lateral 2.04 mm to Lateral 0.96 mm, as referred to in the Paxinos and Franklin mouse brain atlas [25]). The specific expression pattern was assessed with a mix of five antisense probes targeting different regions of Erk4 mRNA. ACB, accumbens nucleus; CA1, CA1 field of the hippocampus; cbgl, cerebellar granular layer; CP, caudate putamen; Cx(LII), cortical layer 2; dcn, deep cerebellar nuclei; Epl, external plexiform layer of the olfactory bulb; grDG, granular layer of the dentate girus; GrO, granule cell layer of the olfactory bulb; icp, inferior cerebellar peduncle; int, internal capsule; LR4V, lateral recess of the fourth ventricle; LV, lateral ventricle; Pir, piriform cortex; Post, posterior subiculum; Pr5, principal sensory trigeminal nucleus; sp5, spinal trigeminal tract; Tu, olfactory tubercle. (B) Representative photographs of hybridization signal in sagittal sections from the brains of $Erk4^{+/+}$ and $Erk4^{-/-}$ mice.

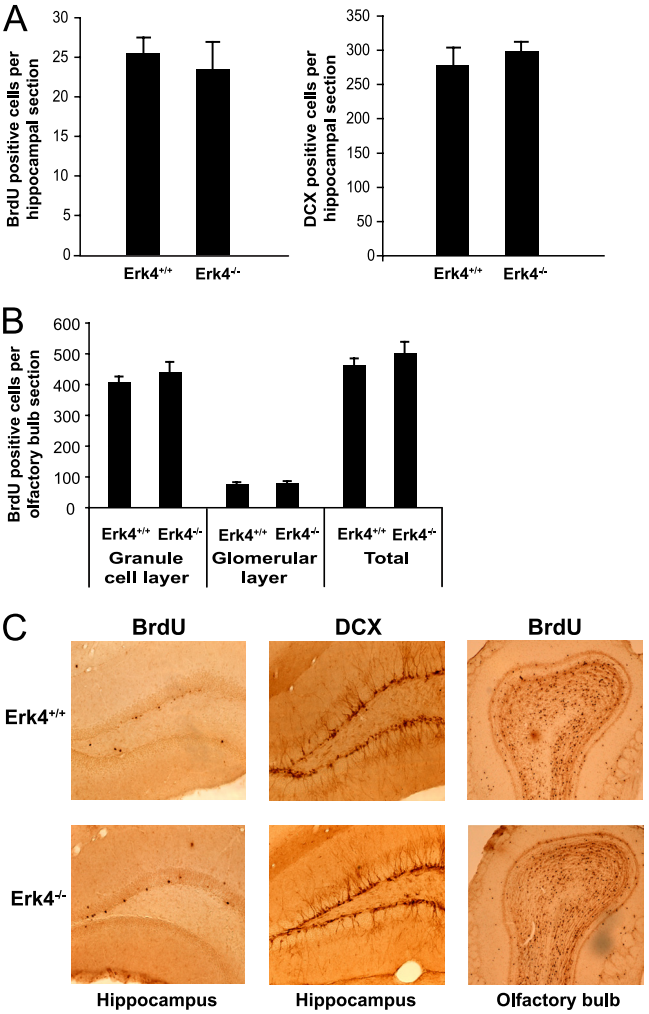

FIG. 5. Loss of Erk4 does not impact on postnatal brain neurogenesis. (A) Quantification of BrdU- and double-cortin (DCX)-positive cells in $Erk4^{+/+}$ and $Erk4^{-/-}$ dentate gyrus of 12-week-old mice. (B) Quantification of BrdU-positive granular and glomerular cells in $Erk4^{+/+}$ and $Erk4^{-/-}$ olfactory bulb. Results are shown as means ± SEMs (n = 5 to 8). (C) Representative images of brain sections from $Erk4^{+/+}$ and $Erk4^{-/-}$ mice stained with BrdU and DCX.

To further test the genetic interaction between Erk3 and Erk4 during embryonic development, we next asked whether additional loss of Erk4 in $Erk3^{-/-}$ mice accentuates Erk3 phenotypes. To address this question, we first repeated the growth and lung maturation analyses in $Erk3^{+/-}$ and $Erk4^{-/-}$; $Erk3^{+/-}$ intercross progeny at E18.5. Since loss of Erk4 has no effect on fetal growth or lung maturation, we intercrossed $Erk4^{-/-}$; $Erk3^{+/-}$ mice instead of $Erk4^{+/-}$; $Erk3^{+/-}$ animals in order to increase the frequency of $Erk4^{-/-}$; $Erk3^{-/-}$ embryos in each litter. When we compared $Erk3^{-/-}$ and $Erk4^{-/-}$; $Erk3^{-/-}$ embryos, we found that additional loss of Erk4 did not further decrease the body weight of Erk3-deficient mice: $Erk3^{-/-}$ mice weighed 0.96 ± 0.03 g, while $Erk4^{-/-}$ $Erk3^{-/-}$ mice weighed 0.95 ± 0.02 g (Fig. 9A). The reduction of body weight in $Erk4^{-/-}$; $Erk3^{-/-}$ mice (17%) was similar to that observed in $Erk3^{-/-}$ embryos (16%) compared to their respective controls (Fig. 9A). We next evaluated the pulmonary immaturity phenotype in E18.5 embryos. We observed a similar decrease in saccular space between double Erk4/Erk3-deficient mice (40%) and Erk3-deficient mice (32%) (Fig. 9B and C). In addition, the increase in the number of type II pneumocytes containing cytoplasmic glycogen granules was not accentuated in $Erk4^{-/-}$; $Erk3^{-/-}$ embryos (2.2-fold) compared to $Erk3^{-/-}$ embryos (2.6-fold) (Fig. 9B and D). Together, these results strongly suggest that intrauterine growth restriction and lung maturation defect are solely due to Erk3 inactivation.

Finally, to determine whether additional loss of Erk4 in $Erk3^{+/-}$ mice may have some incidence on $Erk3^{+/-}$ mouse viability and could mimic the $Erk3^{-/-}$ lethal phenotype, we analyzed the genotype distribution of *Erk4*$^{+/-}$; *Erk3*$^{+/-}$ inter-

TABLE 3. Spontaneous locomotor activity of mice[a]

Mice	Total distance (cm)	Total activity time (s)	Total time for stereotypic movement (s)
$Erk4^{+/+}$	1,992.2 ± 490.1	260.0 ± 67.8	778.0 ± 87.1
$Erk4^{-/-}$	1,516.9 ± 330.6	194.5 ± 47.1	624.9 ± 42.4

[a] Spontaneous locomotor activity was assessed over 60 min. Data are presented as means ± standard errors of the means (SEMs). Distance is shown in centimeters, and time is shown in seconds.

TABLE 4. Motor coordination of mice[a]

Mice	Maximal time on cylinder (s)	Maximal speed (rpm)	Maximal distance (m)
$Erk4^{+/+}$	116.3 ± 8.4	20.2 ± 1.1	2.4 ± 0.3
$Erk4^{-/-}$	112.7 ± 8.7	19.0 ± 1.5	2.2 ± 0.4

[a] The coordination of $Erk4^{+/+}$ and $Erk4^{-/-}$ mice was assessed in a rotarod test. Data are presented as means ± SEMs. Distance is shown in centimeters, speed is shown in rotations per minute, and time is shown in seconds.

TABLE 5. Anxiety-like behavior of mice[a]

Mice	Time spent in open arms (s) in the elevated plus maze	Latent period to begin eating (s) in the Thatcher-Britten test
$Erk4^{+/+}$	33.6 ± 3.8	242.6 ± 17.9
$Erk4^{-/-}$	41.9 ± 5.5	195.6 ± 36.0

[a] Data are presented as means ± SEMs.

cross progeny. Additional loss of one or two alleles of Erk4 did not increase the prevalence of $Erk3^{+/-}$ mouse lethality as confirmed by the presence of $Erk4^{-/-}$; $Erk3^{+/-}$ mice (15%) at the expected Mendelian frequency considering the lethality of $Erk3^{-/-}$ mice (16.7%) (Table 6). Thus, Erk4 is dispensable for mouse embryogenesis, and loss of Erk4 has no impact on the known physiological functions of Erk3.

DISCUSSION

Erk4 and Erk3 are atypical members of the MAP kinase family. Despite their identification more than 15 years ago, the signaling events that control their activity and their physiological functions remain poorly understood. The similar organization of the *Mapk4* and *Mapk6* genes and the high sequence identity of their protein products led us to infer that Erk4 and Erk3 are paralogous proteins (4, 37). Paralogs refer to genes in the same organism that evolved by gene duplication (19). By definition, paralogous proteins experience low evolutionary pressure and their specificity eventually diverges leading to the acquisition of specialized functions. Recently, we have reported that loss of Erk3 leads to intrauterine growth restriction, delayed lung maturation, and neonatal death within the first day of life (18). To investigate the specific physiological function of Erk4, we have generated mice with a targeted disruption of the *Mapk4* gene. Unlike its paralog Erk3, inactivation of Erk4 results in no obvious phenotypic alteration. Erk4-deficient mice are found at the expected Mendelian frequency; they are viable and fertile and display no gross morphological or physiological abnormality. Detailed biochemical characterization indicates that the absence of Erk4 is not compensated by changes in Erk3 expression or activity in embryos and adult tissues.

The highest level of Erk4 expression is detected in mouse brain, raising the possibility that the kinase may play a functional role in specialized neuronal functions. To test this idea, we first determined the spatial distribution pattern of Erk4 mRNA in the adult mouse brain by *in situ* hybridization. In a previous study, Di Benedetto et al. (8) described the mRNA distribution of several components of MAP kinase pathways in the adult mouse brain, including Erk3. However, the expression of Erk4 was not examined in that study. Here, we show that Erk4 mRNA expression is restricted to specific areas of the mouse brain. Interestingly, the regional pattern of Erk4 expression differs from that of Erk3 in several regards. In contrast to Erk4, Erk3 mRNA is weakly expressed in the piriform cortex and is not detected in the olfactory bulb (8). In the

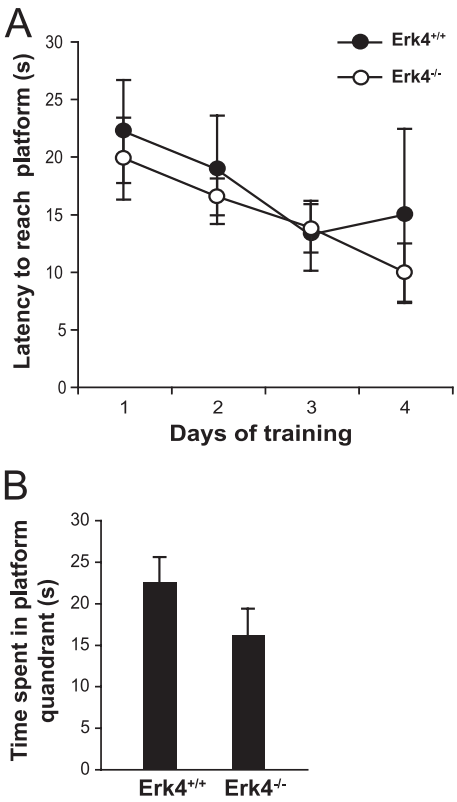

FIG. 6. Normal spatial learning in Erk4-deficient mice. Spatial learning and memory performance were assessed by the Morris water maze test. (A) Time to reach the hidden platform during 4 days of training. (B) Time spent in the target platform quadrant during the probe session. Results are expressed as means ± SEMs (n = 5 to 7).

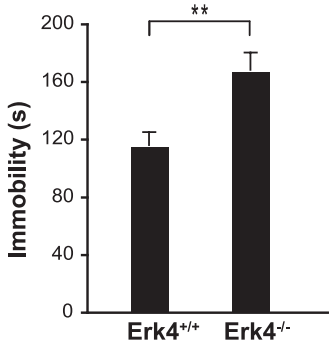

FIG. 7. Erk4-deficient mice manifest depression-related behavior. Mice were analyzed for depression-like phenotype using the forced-swimming test. The immobility time of $Erk4^{-/-}$ mice and wild-type control littermates was recorded during 4 min. Results are presented as means plus SEMs (n = 5 to 7). The values for immobility time of $Erk4^{-/-}$ and $Erk4^{+/+}$ mice are significantly different (**, $P < 0.05$).

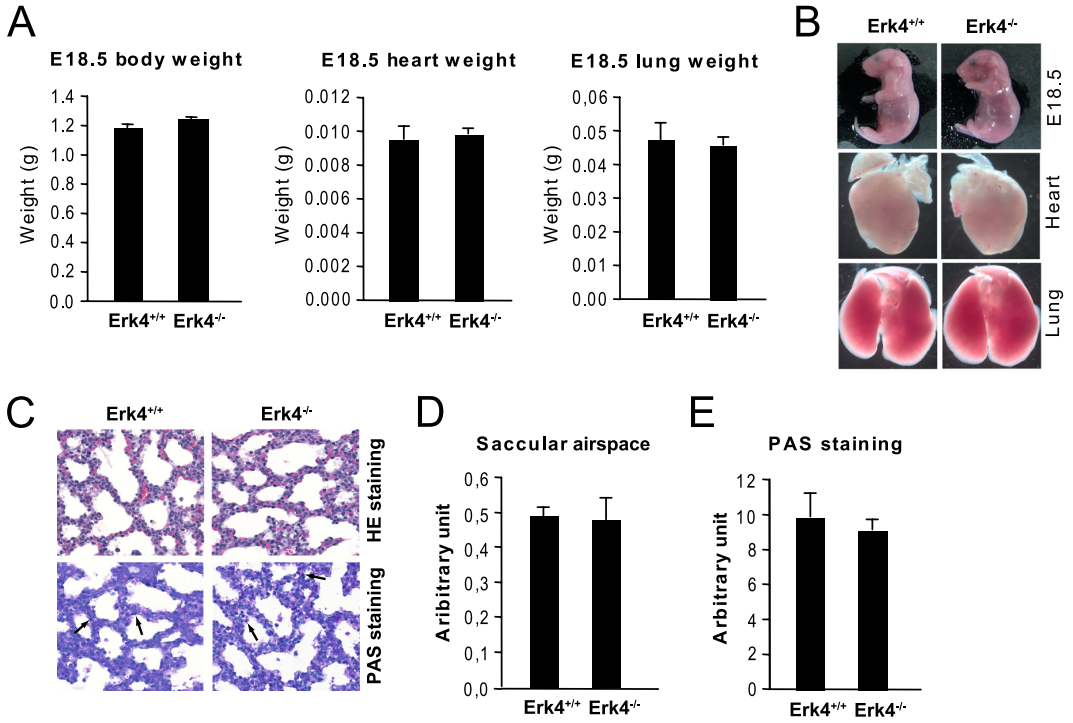

FIG. 8. Loss of Erk4 does not affect intrauterine growth or lung maturation. (A) Body, heart, and lung weights of Erk4$^{+/+}$ and Erk4$^{-/-}$ littermate embryos at E18.5. The mean weight ± SEM for each parameter and genotype follow: body weight, 1.19 ± 0.02 g for *Erk4*$^{+/+}$ embryos (n = 25) and 1.25 ± 0.01 g for *Erk4*$^{-/-}$ embryos (n = 22); heart weight, 0.0096 ± 0.0008 g for *Erk4*$^{+/+}$ embryos (n = 5) and 0.0098 ± 0.0002 g for *Erk4*$^{-/-}$ embryos (n = 11); and lung weight, 0.047 ± 0.005 g for *Erk4*$^{+/+}$ embryos (n = 5) and 0.046 ± 0.002 g for *Erk4*$^{-/-}$ embryos (n = 11). (B) Representative photographs of wild-type and Erk4$^{-/-}$ embryos at E18.5. The whole embryo or the heart and lungs are shown. (C) Representative photographs of lung sections from E18.5 embryos stained with hematoxylin and eosin (HE) or periodic acid-Schiff (PAS). Arrows indicate cytoplasmic glycogen. Magnification, ×40. (D and E) Quantification of lung saccular airspace (D) and PAS staining (E) in Erk4$^{+/+}$ and Erk4$^{-/-}$ embryos (n = 3) at E18.5.

hippocampus, the level of Erk3 is very weak in the CA1 region, and the dentate gyrus is devoid of signal, whereas clear expression of Erk4 is found in these regions. These observations suggest that Erk4 and Erk3 paralogs may have acquired unique functions in the brain as a result of tissue-specific differential expression.

We analyzed the consequences of Erk4 deficiency on motor and behavioral performance of mice. No impairment of locomotion or coordination was observed in Erk4 mutant mice. Since Erk4 mRNA is found in the dentate gyrus and lateral ventricle, we analyzed its function in spatial learning and memory using the Morris water maze test. No effect of Erk4 inactivation was observed in this paradigm. However, as we tested spatial memory only, we cannot exclude the possibility that Erk4 is implicated in other types of learning, such as olfactory or working memory. Erk4-deficient mice did not present significant changes in anxiety-related behavior compared to wild-type littermate controls in two anxiety tests. In accordance with these results, Erk4 mRNA was not detected in the amygdala, a key structure in the anxiety response, or in hypothalamus nuclei involved in the stress response. Interestingly, we observed that Erk4$^{-/-}$ mice spend more time immobile than control animals in the forced-swimming test, an indication of depression-related behavior. The neurogenesis hypothesis of depression (17) is not supported by our data, as we failed to observe any difference in the number of proliferating cells and immature neurons in the hippocampi of Erk4$^{-/-}$ and wild-type mice. The serotonergic system has been widely implicated in the pathogenesis of depression (20). Erk4 mRNA is not detectable in raphe nuclei but is expressed in several projection areas of serotonergic neurons in the cortex, striatum, olfactory tubercle, subiculum, and hippocampus (9). The loss of Erk4 function could also impact on the dopaminergic or noradrenergic system. A monoaminergic depletion could be responsible for the increased despair-like behavior of Erk4-deficient mice.

Paralogy is generally associated with functional diversification. For example, the MAP kinase-activated protein kinase MK2 is the main Hsp27 kinase *in vivo* and plays a major role in the biosynthesis of cytokines (34), whereas the paralog MK5 is involved in oncogenic Ras-induced senescence and skin tumor suppression (36). Another example is the specific function of p38δ isoform in the modulation of insulin secretion and β cell turnover (35). However, paralogs may also retain ancestral functions due to gene dosage effects. One consequence of this genetic redundancy is an increase in genetic robustness against null mutations (12). Functional redundancy of gene duplicates is widespread and is often cited to account for the absence of phenotype in mouse mutants. The inactivation of the *MyoD* and *Myf5* genes involved in myogenesis is a classical example of functional compensation by paralog genes. Loss of MyoD or Myf5 has no impact on muscle development (2, 29), whereas inactivation of both genes results in a complete absence of

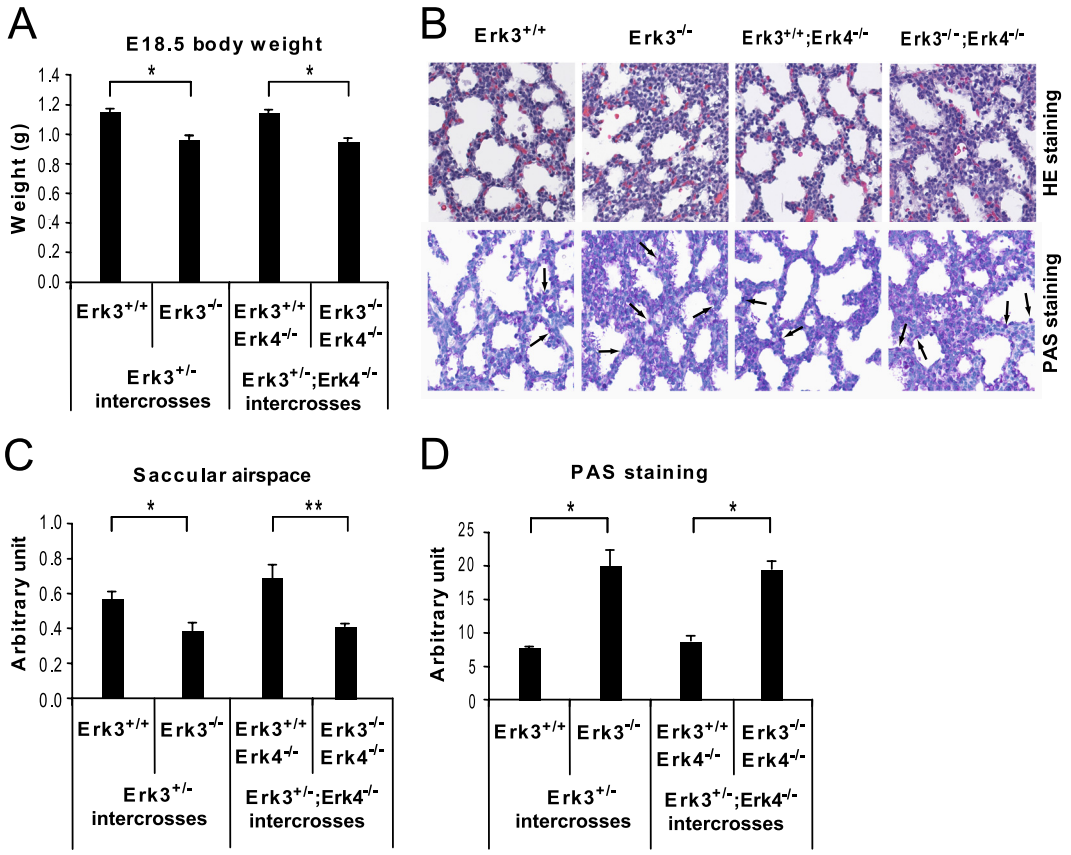

FIG. 9. Additional loss of Erk4 does not accentuate Erk3 intrauterine growth restriction and pulmonary immaturity phenotype of Erk3 mutant mice. (A) Body weight of $Erk3^{+/+}$ embryos, $Erk3^{-/-}$ embryos, $Erk4^{-/-}$; $Erk3^{+/+}$ embryos, and $Erk4^{-/-}$; $Erk3^{-/-}$ embryos at E18.5. The mean body weight ± SEM for each genotype follow: 1.15 ± 0.02 g for $Erk3^{+/+}$ embryos ($n = 22$), 0.96 ± 0.03 g for $Erk3^{-/-}$ embryos ($n = 15$), 1.14 ± 0.02 g for $Erk4^{-/-}$; $Erk3^{+/+}$ embryos ($n = 10$), and 0.95 ± 0.02 g for $Erk4^{-/-}$; $Erk3^{-/-}$ embryos ($n = 24$). The body weight values for $Erk3^{+/+}$ and $Erk3^{-/-}$ embryos are significantly different (*, $P < 0.05$). (B) Representative photographs of lung sections from E18.5 embryos of the indicated genotypes stained with HE or PAS. Arrows indicate cytoplasmic glycogen. Magnification, ×40. (C and D) Quantification of lung saccular airspace (C) and PAS staining (D) in $Erk3^{+/+}$ embryos, $Erk3^{-/-}$ embryos, $Erk4^{-/-}$; $Erk3^{+/+}$ embryos, and $Erk4^{-/-}$; $Erk3^{-/-}$ embryos at E18.5 ($n = 5$ to 7). The saccular airspace and PAS staining values for $Erk3^{+/+}$ and $Erk3^{-/-}$ embryos are significantly different: *, $P < 0.05$; **, $P < 0.001$.

TABLE 6. Genotype analysis of the progeny from $Erk4^{+/-}$; $Erk3^{+/-}$ intercrosses[a]

Genotype of progeny mice	Frequency (%) of progeny with the observed genotype	Expected genotype frequency (%)[b]
Erk4$^{+/+}$;		
Erk3$^{+/+}$	7	8.33 (6.25)
Erk3$^{+/-}$	18	16.66 (12.5)
Erk3$^{-/-}$	0	0 (6.25)
Erk4$^{+/-}$;		
Erk3$^{+/+}$	13	16.66 (12.5)
Erk3$^{+/-}$	36	33.33 (25)
Erk3$^{-/-}$	0	0 (12.5)
Erk4$^{-/-}$;		
Erk3$^{+/+}$	11	8.33 (6.25)
Erk3$^{+/-}$	15	16.66 (12.5)
Erk3$^{-/-}$	0	0 (6.25)

[a] Progeny with C57BL/6J-129/Sv mixed genetic background ($n = 100$).
[b] Frequencies expected considering Erk3 null mice lethality. The Mendelian inheritance frequencies are shown in the parentheses.

skeletal muscles (30). The overlapping pattern of Erk4 and Erk3 expression in tissues of the developing mouse embryo (15) is consistent with the idea that the two kinases may exert some redundant functions. To ask whether Erk4 and Erk3 functionally overlap, we analyzed the phenotype of compound mutant mice. Our results indicate that Erk4 and Erk3 do not exhibit genetic interactions under the controlled physiological conditions tested in this study. First, Erk3 expression or activity is not upregulated in tissues of Erk4-deficient mice. Second, Erk4 inactivation does not aggravate the fetal growth and lung maturation phenotypes of Erk3 mutant mice. Third, loss of Erk4 does not lead to neonatal lethality of $Erk3^{+/-}$ mice, and no additional phenotype is observed in mice lacking both Erk4 and Erk3.

Phenotypic differences of paralog-deficient mice are a good indication of specialized functions *in vivo*, but inactivation of both genes is required to fully address the question. For example, inactivation of Erk1 does not result in any developmental defect (24), whereas conditional inactivation of Erk2 in the neural crest results in craniofacial and conotruncal cardiac embryonic defects (23), suggesting that Erk1 and Erk2 exert

nonredundant functions in neural crest development. However, additional mutation of Erk1 revealed that Erk2 neural crest-derived phenotypes are accentuated by the loss of Erk1 in a dose-dependent manner (23). Thus, the distinct phenotypes of Erk1 and Erk2 mutant mice are rather due to Erk2 compensation than to Erk2 specific function in neural crest development. The results presented here demonstrate that Erk3 and Erk4 have acquired specialized functions through evolutionary diversification. However, we cannot exclude the possibility that Erk3 and Erk4 may exhibit partial genetic redundancy under different environmental conditions or under cellular stresses. Further studies will be required to test this idea.

Genetic studies of *Saccharomyces cerevisiae* have provided evidence that diversification of paralogs is often asymmetrical with one member of the gene pair acquiring more complex regulatory mechanisms and protein-protein interactions than the other (40). Despite their similarities, Erk3 and Erk4 show distinct structural and regulatory properties. First, Erk3 and Erk4 share 73% amino acid identity in the kinase domain, but this similarity decreases to 31% in the C-terminal region with Erk3 having 137 additional amino acids. Second, Erk4 is a stable protein, whereas Erk3 is unstable being constitutively degraded by the ubiquitin-proteasome pathway (1, 5, 15). Third, Erk3 and Erk4 exhibit distinct subcellular localization in various cell types (1, 14). From our analysis, we conclude that the functions of Erk3 and Erk4 paralogs have diverged since duplication of their original ancestor gene and that Erk4 is dispensable for mouse development under normal physiological conditions.

ACKNOWLEDGMENTS

We gratefully acknowledge the scientific contributions of many colleagues, with special thanks to P. Coulombe and M. Saba-El-Leil. We also thank K. Lévesque for outstanding technical assistance, E. M. Charbonneau and J. Rochford for advice on behavioral testing, L. Gaboury for histopathological analysis, and the staff of the IRIC histology and genomic facilities.

N. Cermakian is supported by a Fonds de la Recherche en Santé du Québec salary award. S. Meloche holds the Canada Research Chair in Cellular Signaling. This work was supported by grants from the Canadian Institutes for Health Research (S.M.) and the Natural Science and Engineering Research Council (N.C.).

REFERENCES

1. **Aberg, E., M. Perander, B. Johansen, C. Julien, S. Meloche, S. M. Keyse, and O. M. Seternes.** 2006. Regulation of MAPK-activated protein kinase 5 activity and subcellular localization by the atypical MAPK ERK4/MAPK4. J. Biol. Chem. **281:**35499–35510.
2. **Braun, T., M. A. Rudnicki, H. H. Arnold, and R. Jaenisch.** 1992. Targeted inactivation of the muscle regulatory gene Myf-5 results in abnormal rib development and perinatal death. Cell **71:**369–382.
3. **Cameron, H. A., and R. McKay.** 1998. Stem cells and neurogenesis in the adult brain. Curr. Opin. Neurobiol. **8:**677–680.
4. **Coulombe, P., and S. Meloche.** 2007. Atypical mitogen-activated protein kinases: structure, regulation and functions. Biochim. Biophys. Acta **1773:**1376–1387.
5. **Coulombe, P., G. Rodier, S. Pelletier, J. Pellerin, and S. Meloche.** 2003. Rapid turnover of extracellular signal-regulated kinase 3 by the ubiquitin-proteasome pathway defines a novel paradigm of mitogen-activated protein kinase regulation during cellular differentiation. Mol. Cell. Biol. **23:**4542–4558.
6. **Cuenda, A., and S. Rousseau.** 2007. p38 MAP-kinases pathway regulation, function and role in human diseases. Biochim. Biophys. Acta **1773:**1358–1375.
7. **Deleris, P., J. Rousseau, P. Coulombe, G. Rodier, P. L. Tanguay, and S. Meloche.** 2008. Activation loop phosphorylation of the atypical MAP kinases ERK3 and ERK4 is required for binding, activation and cytoplasmic relocalization of MK5. J. Cell. Physiol. **217:**778–788.
8. **Di Benedetto, B., C. Hitz, S. M. Holter, R. Kuhn, D. M. Vogt Weisenhorn, and W. Wurst.** 2007. Differential mRNA distribution of components of the ERK/MAPK signalling cascade in the adult mouse brain. J. Comp. Neurol. **500:**542–556.
9. **Frazer, A., and J. G. Hensler.** 1999. Understanding the neuroanatomical organization of serotonergic cells in the brain provides insight into the functions of this neurotransmitter, 6th ed. Lippincott-Raven, Philadelphia, PA.
10. **Gonzalez, F. A., D. L. Raden, M. R. Rigby, and R. J. Davis.** 1992. Heterogeneous expression of four MAP kinase isoforms in human tissues. FEBS Lett. **304:**170–178.
11. **Gras, C., B. Amilhon, E. M. Lepicard, O. Poirel, J. Vinatier, M. Herbin, S. Dumas, E. T. Tzavara, M. R. Wade, G. G. Nomikos, N. Hanoun, F. Saurini, M. L. Kemel, B. Gasnier, B. Giros, and S. El Mestikawy.** 2008. The vesicular glutamate transporter VGLUT3 synergizes striatal acetylcholine tone. Nat. Neurosci. **11:**292–300.
12. **Gu, Z., L. M. Steinmetz, X. Gu, C. Scharfe, R. W. Davis, and W. H. Li.** 2003. Role of duplicate genes in genetic robustness against null mutations. Nature **421:**63–66.
13. **Hayashi, M., and J. D. Lee.** 2004. Role of the BMK1/ERK5 signaling pathway: lessons from knockout mice. J. Mol. Med. **82:**800–808.
14. **Julien, C., P. Coulombe, and S. Meloche.** 2003. Nuclear export of ERK3 by a CRM1-dependent mechanism regulates its inhibitory action on cell cycle progression. J. Biol. Chem. **278:**42615–42624.
15. **Kant, S., S. Schumacher, M. K. Singh, A. Kispert, A. Kotlyarov, and M. Gaestel.** 2006. Characterization of the atypical MAPK ERK4 and its activation of the MAPK-activated protein kinase MK5. J. Biol. Chem. **281:**35511–35519.
16. **Karl, T., R. Pabst, and S. von Horsten.** 2003. Behavioral phenotyping of mice in pharmacological and toxicological research. Exp. Toxicol. Pathol. **55:**69–83.
17. **Kempermann, G., and G. Kronenberg.** 2003. Depressed new neurons–adult hippocampal neurogenesis and a cellular plasticity hypothesis of major depression. Biol. Psychiatry **54:**499–503.
18. **Klinger, S., B. Turgeon, K. Levesque, G. A. Wood, K. M. Aagaard-Tillery, and S. Meloche.** 2009. Loss of Erk3 function in mice leads to intrauterine growth restriction, pulmonary immaturity, and neonatal lethality. Proc. Natl. Acad. Sci. U. S. A. **106:**16710–16715.
19. **Koonin, E. V.** 2005. Orthologs, paralogs, and evolutionary genomics. Annu. Rev. Genet. **39:**309–338.
20. **Meltzer, H. Y.** 1990. Role of serotonin in depression. Ann. N. Y. Acad. Sci. **600:**486–500.
21. **Morris, R.** 1984. Developments of a water-maze procedure for studying spatial learning in the rat. J. Neurosci. Methods **11:**47–60.
22. **Nagy, A., J. Rossant, R. Nagy, W. Abramow-Newerly, and J. C. Roder.** 1993. Derivation of completely cell culture-derived mice from early-passage embryonic stem cells. Proc. Natl. Acad. Sci. U. S. A. **90:**8424–8428.
23. **Newbern, J., J. Zhong, R. S. Wickramasinghe, X. Li, Y. Wu, I. Samuels, N. Cherosky, J. C. Karlo, B. O'Loughlin, J. Wikenheiser, M. Gargesha, Y. Q. Doughman, J. Charron, D. D. Ginty, M. Watanabe, S. C. Saitta, W. D. Snider, and G. E. Landreth.** 2008. Mouse and human phenotypes indicate a critical conserved role for ERK2 signaling in neural crest development. Proc. Natl. Acad. Sci. U. S. A. **105:**17115–17120.
24. **Pages, G., S. Guerin, D. Grall, F. Bonino, A. Smith, F. Anjuere, P. Auberger, and J. Pouyssegur.** 1999. Defective thymocyte maturation in p44 MAP kinase (Erk 1) knockout mice. Science **286:**1374–1377.
25. **Paxinos, G., and K. B. J. Franklin.** 2001. The mouse brain in stereotaxic coordinates, 2nd ed. Academic Press, San Diego, CA.
26. **Pearson, G., F. Robinson, T. Beers Gibson, B. E. Xu, M. Karandikar, K. Berman, and M. H. Cobb.** 2001. Mitogen-activated protein (MAP) kinase pathways: regulation and physiological functions. Endocr. Rev. **22:**153–183.
27. **Pfaffl, M. W.** 2001. A new mathematical model for relative quantification in real-time RT-PCR. Nucleic Acids Res. **29:**e45.
28. **Rochford, J., S. Beaulieu, I. Rousse, J. R. Glowa, and N. Barden.** 1997. Behavioral reactivity to aversive stimuli in a transgenic mouse model of impaired glucocorticoid (type II) receptor function: effects of diazepam and FG-7142. Psychopharmacology **132:**145–152.
29. **Rudnicki, M. A., T. Braun, S. Hinuma, and R. Jaenisch.** 1992. Inactivation of MyoD in mice leads to up-regulation of the myogenic HLH gene Myf-5 and results in apparently normal muscle development. Cell **71:**383–390.
30. **Rudnicki, M. A., P. N. Schnegelsberg, R. H. Stead, T. Braun, H. H. Arnold, and R. Jaenisch.** 1993. MyoD or Myf-5 is required for the formation of skeletal muscle. Cell **75:**1351–1359.
31. **Schumacher, S., K. Laass, S. Kant, Y. Shi, A. Visel, A. D. Gruber, A. Kotlyarov, and M. Gaestel.** 2004. Scaffolding by ERK3 regulates MK5 in development. EMBO J. **23:**4770–4779.
32. **Servant, M. J., P. Coulombe, B. Turgeon, and S. Meloche.** 2000. Differential regulation of p27(Kip1) expression by mitogenic and hypertrophic factors: involvement of transcriptional and posttranscriptional mechanisms. J. Cell Biol. **148:**543–556.
33. **Seternes, O. M., T. Mikalsen, B. Johansen, E. Michaelsen, C. G. Armstrong, N. A. Morrice, B. Turgeon, S. Meloche, U. Moens, and S. M. Keyse.** 2004.

Activation of MK5/PRAK by the atypical MAP kinase ERK3 defines a novel signal transduction pathway. EMBO J. **23:**4780–4791.

34. **Shi, Y., A. Kotlyarov, K. Laabeta, A. D. Gruber, E. Butt, K. Marcus, H. E. Meyer, A. Friedrich, H. D. Volk, and M. Gaestel.** 2003. Elimination of protein kinase MK5/PRAK activity by targeted homologous recombination. Mol. Cell. Biol. **23:**7732–7741.
35. **Sumara, G., I. Formentini, S. Collins, I. Sumara, R. Windak, B. Bodenmiller, R. Ramracheya, D. Caille, H. Jiang, K. A. Platt, P. Meda, R. Aebersold, P. Rorsman, and R. Ricci.** 2009. Regulation of PKD by the MAPK p38delta in insulin secretion and glucose homeostasis. Cell **136:**235–248.
36. **Sun, P., N. Yoshizuka, L. New, B. A. Moser, Y. Li, R. Liao, C. Xie, J. Chen, Q. Deng, M. Yamout, M. Q. Dong, C. G. Frangou, J. R. Yates III, P. E. Wright, and J. Han.** 2007. PRAK is essential for ras-induced senescence and tumor suppression. Cell **128:**295–308.
37. **Turgeon, B., B. F. Lang, and S. Meloche.** 2002. The protein kinase ERK3 is encoded by a single functional gene: genomic analysis of the ERK3 gene family. Genomics **80:**673–680.
38. **Turgeon, B., M. K. Saba-El-Leil, and S. Meloche.** 2000. Cloning and characterization of mouse extracellular-signal-regulated protein kinase 3 as a unique gene product of 100 kDa. Biochem. J. **346:**169–175.
39. **Voisin, L., M. K. Saba-El-Leil, C. Julien, C. Fremin, and S. Meloche.** 2010. Genetic demonstration of a redundant role of extracellular signal-regulated kinase 1 (ERK1) and ERK2 mitogen-activated protein kinases in promoting fibroblast proliferation. Mol. Cell. Biol. **30:**2918–2932.
40. **Wagner, A.** 2002. Asymmetric functional divergence of duplicate genes in yeast. Mol. Biol. Evol. **19:**1760–1768.
41. **Weston, C. R., and R. J. Davis.** 2007. The JNK signal transduction pathway. Curr. Opin. Cell Biol. **19:**142–149.